NeuroImage 152 (2017) 381–389

Contents lists available at ScienceDirect

NeuroImage

journal homepage: www.elsevier.com/locate/neuroimage

Interactions between the anterior cingulate-insula network and the fronto-parietal network during perceptual decision-making

Ganesh B. Chand[a,b,*], Mukesh Dhamala[c,d]

[a] Department of Physics and Astronomy, Georgia State University, Atlanta, GA 30303, USA
[b] Department of Medicine, Emory University School of Medicine, Atlanta, GA 30329, USA
[c] Neuroscience Institute, Georgia State University, Atlanta, GA 30303, USA
[d] Center for Behavioral Neuroscience, Center for Nano-Optics, Center for Diagnostics and Therapeutics, GSU-GaTech Center for Advanced Brain Imaging, Georgia State University, Atlanta, GA 30303, USA

ARTICLE INFO

Keywords:
Beta oscillation
Gamma oscillation
Large-scale networks
EEG source reconstruction
Granger causality

ABSTRACT

Information processing in the human brain during cognitively demanding goal-directed tasks is thought to involve several large-scale brain networks, including the anterior cingulate-insula network (aCIN) and the fronto-parietal network (FPN). Recent functional MRI (fMRI) studies have provided clues that the aCIN initiates activity changes in the FPN. However, when and how often these networks interact remains largely unknown to date. Here, we systematically examined the oscillatory interactions between the aCIN and the FPN by using the spectral Granger causality analysis of reconstructed brain source signals from the scalp electroencephalography (EEG) recorded from human participants performing a face-house perceptual categorization task. We investigated how the aCIN and the FPN interact, what the temporal sequence of events in these nodes is, and what frequency bands of information flow bind these nodes in networks. We found that beta band (13–30 Hz) and gamma (30–100 Hz) bands of interactions are involved between the aCIN and the FPN during decision-making tasks. In gamma band, the aCIN initiated the Granger causal control over the FPN in 25–225 ms timeframe. In beta band, the FPN achieved a control over the aCIN in 225–425 ms timeframe. These band-specific time-dependent Granger causal controls of the aCIN and the FPN were retained for behaviorally harder decision-making tasks. These findings of times and frequencies of oscillatory interactions in the aCIN and FPN provide us new insights into the general neural mechanisms for sensory information-guided, goal-directed behaviors, including perceptual decision-making processes.

Introduction

Previous neuroimaging investigations have described large-scale, intrinsically organized brain networks underlying a broad range of brain functions, from sensory to motor and to higher-level cognitive functions (Deco et al., 2011; Power et al., 2011; Seeley et al., 2007). The anterior cingulate-insula network (aCIN) and the fronto-parietal network (FPN) are known to be central for cognitive functions (Chen et al., 2013; Uddin, 2015). Functional magnetic resonance imaging (fMRI) studies (Goulden et al., 2014; Sridharan et al., 2008) have demonstrated that the aCIN sends a dominant information flow to the FPN in goal-directed tasks. However, what remains poorly understood is how these networks interact in the time-scales of human cognitive processes.

The individual functional roles of the brain areas in the aCIN have not been precisely resolved. The dorsal anterior cingulate cortex (DACC) of aCIN is known to monitor performance, to signal the need for behavioral adaptation (Ridderinkhof et al., 2004), and in concert with the lateral prefrontal cortex to signal enhanced cognitive control and implement behavioral changes (Egner, 2009; Ridderinkhof et al., 2004). The anterior insula (AI), especially the right AI (R AI), is known as cortical outflow hub of the aCIN to coordinate a change in activity across multiple brain networks, including the FPN (Bonnelle et al., 2012; Menon and Uddin, 2010; Sridharan et al., 2008). Here, we seek to examine the interactions between the aCIN and the FPN in millisecond time-scale. Since multiple frequency bands of neural oscillations have important implications for cognitive processes (Diener et al., 2012; Hipp et al., 2011; Siegel et al., 2012), we also seek to examine the spectra of information flow between the aCIN and the FPN during perceptual decision-making.

We performed electroencephalography (EEG) experiments by using clear and degraded face-house images in perceptual categorization

* Correspondence to: Department of Physics and Astronomy, Georgia State University, 1 Park Place NE, Suite 439B, Atlanta, GA 30303, USA. .
E-mail address: gchand1@student.gsu.edu (G.B. Chand).

http://dx.doi.org/10.1016/j.neuroimage.2017.03.014
Received 10 December 2016; Accepted 7 March 2017
Available online 08 March 2017

task. We reconstructed waveforms of EEG sources associated with perceptual decisions and applied spectral Granger causality methods (Dhamala et al., 2008a; Dhamala et al., 2008b) to examine at the frequency-specific network interactions between the aCIN and the FPN. We hypothesized that the FPN would be under Granger causal control from the aCIN, this causal influence would change during a course of a perceptual decision, and this casual influence would be retained by the task difficulty.

Materials and methods

Participants

In this study, 26 human volunteers (21 males, 5 females) of age ranged from 22 to 38 years (mean: 26.3 years, standard deviation: 4.7 years) participated. Each participant reported that he or she is not currently on medication for mental illness or had a prior history of mental illness affecting decision-making abilities. Out of 26 participants, 4 participants reported that they are left-handed. We collected a written informed consent from each participant prior to the data collection. The Institutional Review Board of Georgia State University approved this experimental protocol. We excluded three participants from the final analyses because of unmanageable artifacts in their EEG data and/or very low behavior performance.

Stimuli

Total 28 images of faces and houses (14 images of each category) were used. Face images were taken from the Ekman series (Ekman and Friesen, 1976). Fast Fourier transforms (FFT) of these images were computed, which provided 28 magnitude and twenty-eight phase matrices. Images were produced from the inverse FFT (IFFT) of average magnitude matrix and individual phase matrices, where phase matrix was a linear combination of the original phase matrix computed during the forward Fourier transforms and a random Gaussian noise matrix. The resulting images had an identical frequency power spectrum (corresponding to the average magnitude matrix) and had graded percent of noise as performed in the previous study (Heekeren et al., 2004; Heekeren et al., 2008). Thus, the stimuli consisted of three different noise-levels: 0%, 40% and 55% (i.e., clear stimuli, 40% noisy stimuli, and 55% noisy stimuli). We used E-Prime 2.0 software to display the task sequence.

Experimental design

The participants were briefly explained about the task paradigm before the experiment. Participant sat in a dark room and a viewing distance was about 60 cm from their chin. Fig. 1 shows a schematic of experiment. It consisted of 4 blocks of 168 trials (672 trials in total with 224 trials for each noise-level). A small fixation cross ('+') was displayed in the middle of the computer screen for 500 ms, stimulus was then showed for 150 ms, and a black background with question mark ('?') was displayed for 1500 ms. The participants were allowed to indicate their decision (either face or house) by keyboard press during question mark time. The responses made after that delay were considered incorrect and were excluded.

Data acquisition and preprocessing

We acquired EEG data using 64-channel EEG system of Brain Vision LLC (http://www.brainvision.com). Analog signal was digitized at 500 Hz and each electrode impedance was maintained below 10 kΩ. The participants were asked to minimize blinking, head movements, and swallowing. Data were band-pass filtered between 1 Hz and 100 Hz, and notch filtered to remove 60 Hz AC-line noises. Independent component analysis (ICA)-based ocular correction of

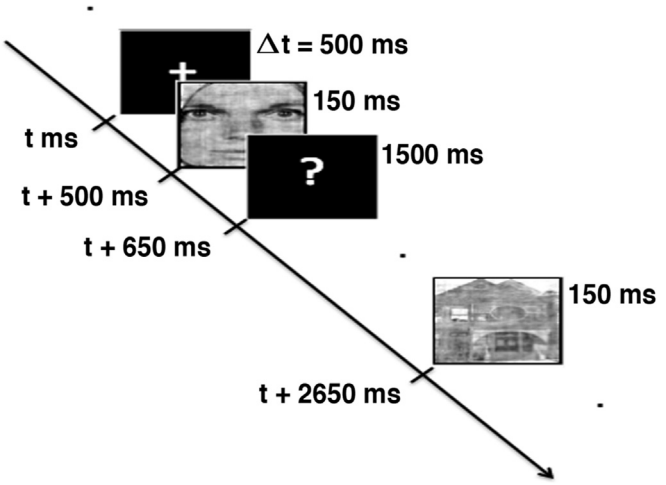

Fig. 1. Experimental sequence design: Stimulus was presented for 150 ms, followed by question mark ('?') for 1500 ms to respond whether image is a face or house.

Brain Vision Analyzer 2.0 (http://www.brainproducts.com) was used to remove the eyes blinking artifacts.

Data analysis

The EEG data analysis consists of the following major steps:

(1) *Event related potentials (ERPs)*: Continuous EEG data were segmented into trials of 425 ms duration (post-stimulus: 0 to 425 ms) based on the stimulus onset time. Trials that correspond to the correct responses were separated. The trials that had three standard deviations below or above the global mean across time in each subject were considered as outliers (Junghofer et al., 2000) and were discarded.

(2) *EEG-source and single-trials source waveforms reconstruction*: All correct response trials were grand averaged and imported to BESA software version 5.3.7 (www.besa.de) to reconstruct EEG sources. Individual structural MRI was not recorded. We used the low resolution electromagnetic tomography (LORETA) (Pascual-Marqui et al., 1994) to estimate the localized sources. LORETA has been widely used in EEG source reconstruction for cortical and subcortical structures, including insula and hippocampus (Clemens et al., 2010; Herrmann et al., 2005; Jones and Bhattacharya, 2012; Thatcher et al., 2014; Velikova et al., 2010). LORETA improves the problem of surface-restricted localization methods (Michel et al., 2004; Painold et al., 2011; Pascual-Marqui et al., 1999). LORETA computes inverse solution at 2394 voxels with spatial resolutions of 7 mm in the Talairach atlas (Pascual-Marqui et al., 1999; Pascual-Marqui et al., 1994). It assumes that the smoothest of all possible neural activity distributions is the most plausible one, which is also supported by electrophysiology. Electrophysiology suggests that neighboring neuronal populations show highly correlated activity while EEG-LORETA results are the activity rendered by neighboring voxels with maximally similar activity (Haalman and Vaadia, 1997; Herrmann et al., 2005; Michel et al., 2004). Functionally very distinct brain areas can be anatomically very close such as the medial parts of the two hemispheres. However, LORETA sometimes can produce the results that encompass the two hemispheres providing inevitable mixing of sources. The results should therefore interpret with caution in such case. Locations of sources can be constrained to the cortical surface and their orientations perpendicular to the local cortical surface based on neurophysiological information that the sources of EEG are postsynaptic currents in cortical pyramidal cell, and that the direction of these currents is perpendicular to the

Table 1
The anatomical locations, dominant activation timeframes of localized sources for correctly perceived stimuli, and orientations of fitted dipoles at those sources.

Brain areas	Talairach coordinates (mm) x, y, z	Dipole orientations x, y, z	Dominant activation period (ms)
Visual area (V_1)	-6, −74, −6	−0.1, −1.0, −0.3	50 – 65
Posterior parietal cortex (PPC)	4.0, −52.0, 31.0	0.1, −0.8, 0.6	65 – 85
Right anterior insula (R AI)	35.0, 9.0, −7.0	0.9, 0.3, −0.4	78 – 142
Left anterior insula (L AI)	−33.0, 11.0, −8.0	−0.9, 0.4, −0.3	76 – 144
Dorsal anterior cingulate cortex (DACC)	4.0, 38.0, 13.0	0.1, 1.0, 0.0	76 – 146
Fusiform face area (FFA)	36.0, −47.0, −16.0	0.6, −0.7, −0.4	140 – 190
Para-hippocampal place area (PPA)	−30.0, −45.0, −10.0	−0.5, −0.8, −0.3	145 – 200
Dorsolateral prefrontal cortex (DLPFC)	−21.0, 39.0, 28.0	−0.3, 0.9, 0.4	210 – 245

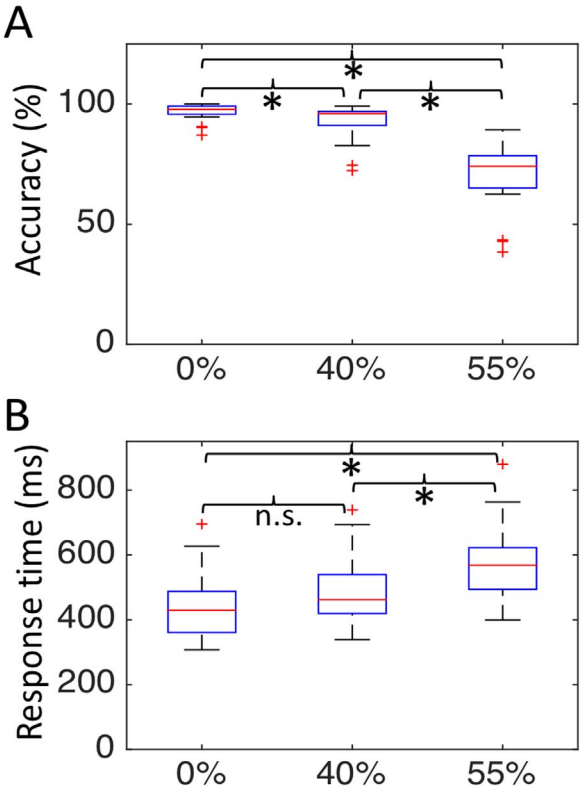

Fig. 2. Behavioral responses. A) Behavioral accuracy (%) significantly decreased, but B) response time (milliseconds) significantly increased with the increase in noise in the stimuli. (*: p < 0.001; FDR-corrected; n.s.: not significant).

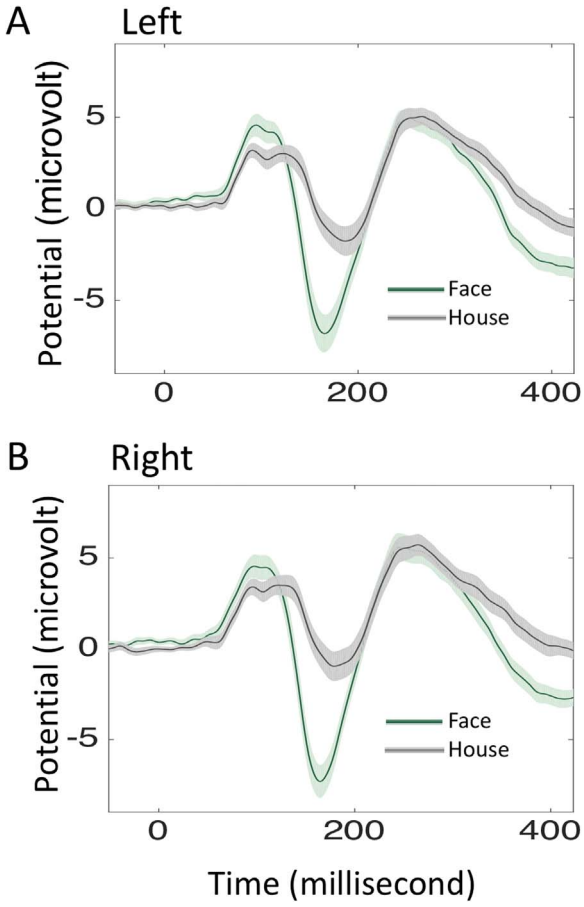

Fig. 3. ERPs over the occipital-temporal channels in the left hemisphere (A) and right hemisphere (B) (shaded region indicates the standard error of mean (SEM) over subjects).

cortical surface (Dale and Sereno, 1993; Hämäläinen et al., 1993). We fitted dipoles at all locations of peak activation–the R AI, left AI (L AI), and DACC of aCIN, the dorsolateral prefrontal cortex (DLPFC) and posterior parietal cortex (PPC) of FPN, the lower visual area (V_1), the fusiform face area (FFA) and para-hippocampal place area (PPA) of ventral-temporal cortex with dipole orientations shown in Table 1. The single-trial source signals were extracted using a four-shell spherical head model and a regularization constant of 1% for the inverse operator as performed in the previous investigations (Adhikari et al., 2014; Chand and Dhamala, 2016b; Chand et al., 2016). The source signals were subsequently used for the spectral power and Granger causality calculations.

(3) *Spectral power and Granger causality*: Using single-trial source signals, power spectra (Chand and Dhamala, 2014; Dhamala et al., 2008a; Dhamala et al., 2008b) can be calculated using parametric and nonparametric methods. We have chosen to use Granger causality method although other methods such as directed transfer function, partial directed coherence, and dynamic causal modeling can achieve similar goals (Dhamala, 2014). Granger causality is a data-driven technique and relies on fewer assumptions about the underlying interactions and dynamics. Granger causality is also computationally less intensive than technique like dynamical causal modeling. Our recent study also indicates that, if applied appropriately, both Granger causality and dynamical causal modeling can yield the consistent results (Bajaj et al., 2016). Granger causality can be computed to examine the strengths, directions, and frequencies of interactions between dynamic processes. In frequency (f) domain, Granger causality from the second time series X_2 to the first time series X_1 (i.e., node 2 to node 1) is calculated as (Chand and Dhamala, 2016b; Dhamala et al., 2008a; Dhamala et al., 2008b),

$$M_{2\to1}(f) = -\ln\left(1 - \frac{(\sum_{22} - \sum_{12}^2 - \sum_{11})|H_{12}(f)|^2}{S_{11}(f)}\right) \quad (1)$$

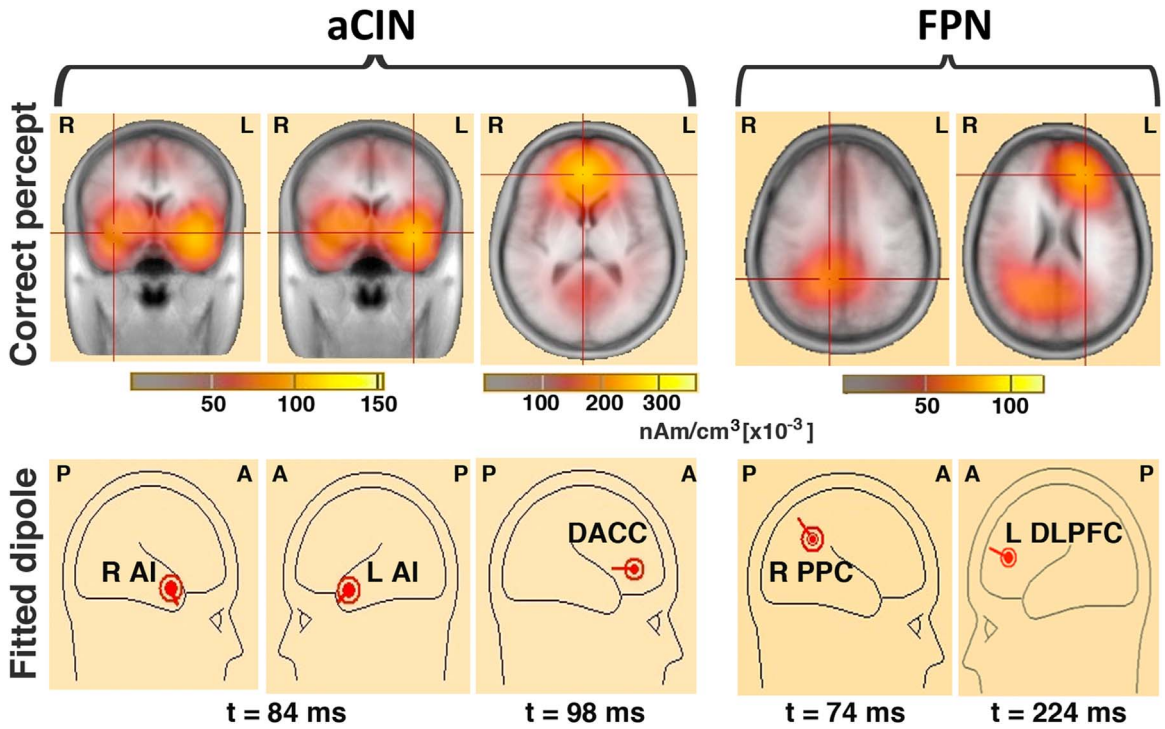

Fig. 4. Spatiotemporal profiles of peak source-level brain activity at the nodes of anterior cingulate-insula network (aCIN) and fronto-parietal network (FPN). The first row shows peak source-level brain activity over the right anterior insula (R AI) and left anterior insula (L AI) at ~84 ms, dorsal anterior cingulate cortex (DACC) at ~98 ms, posterior parietal cortex (PPC) at ~74 ms and dorsolateral prefrontal cortex (DLPFC) at ~224 ms, and the second row shows fitted dipoles on those nodes.

Where S is spectral power, H is transfer function, and ∑ is noise covariance. The value of Granger causality (M) ranges from 0 to +∞.

For 'N' EEG-sources, the frequency-specific Granger causal outflow (F) at a node i can be defined as:

$$F_i = \frac{1}{N-1}\sum_{j}^{N}(M_{i\to j} - M_{j\to i}) \quad (2)$$

Here, we have three nodes of aCIN and two nodes of FPN so j can be 1, 2, 3, 4 and 5. If we assign, for example, the R AI = 1 (first node), DACC = 2 (second node), L AI = 3 (third node), DLPFC = 4 (fourth node), and PPC = 5 (fifth node) then Granger causal outflow of the R AI is $F_1 = [(M_{1->2} - M_{2->1}) + (M_{1->3} - M_{3->1}) + (M_{1->4} - M_{4->1}) + (M_{1->5} - M_{5->1})]/4$, where $M_{1->2}$ is Granger causality from the first node to second node, and $M_{2->1}$ is Granger causality from the second node to first node. Similarly, we compute Granger causal outflows of the DACC, L AI, DLPFC, and PPC nodes.

The spectral power was computed using the parametric spectral approach (Chand and Dhamala, 2014; Dhamala et al., 2008a; Dhamala et al., 2008b) from the source waveforms of aCIN and FPN nodes in two consecutive timeframes: 25 ms to 225 ms and 225 ms to 425 ms. Model order (= 4) was selected by comparing the spectral power from both parametric and nonparametric approaches (Dhamala et al., 2008a) at different model orders and by picking the model order that gave the lowest power difference between two approaches. The Granger causality was computed from source waveforms of the nodes. We also computed Granger causality spectra using a sliding time window approach (Cui et al., 2008; Ding et al., 2000), and further calculated outflow to cross validate our results.

Results

Behavioral results

The overall accuracy percent is defined as the ratio of the number of correctly responded trials to the total number of presented trials multiplied by hundred. The accuracy percent was significantly higher for 0% noise compared with that of 40% and 55% noises. The average response times for 0%, 40%, and 55% noisy stimuli were 434.02 ms, 484.28 ms, and 565.70 ms, respectively. We limited our analysis (electrophysiological results below) within 425 ms to exclude the possibility of finger movement related artifacts during the response period. The comparison between noise levels were assessed using Wilcoxon rank sum followed by (false discovery rate) correction (see Fig. 2).

Electrophysiological results

Event related potentials (ERPs)

Average ERPs for correct responses were computed to examine the ERP features over occipital-temporal electrodes (Fig. 3). We found first negative peak at ~170 ms, often known as N170-component as in previous studies of face perception (Nguyen et al., 2014; Rousselet et al., 2008). The ERPs over the right occipital-temporal channels (P_6, P_8 and PO_8) and the left occipital-temporal channels (P_5, P_7 and PO_7) showed relatively right and left lateralized activity for faces and houses, respectively. ERPs for faces are relatively higher than those for houses.

Temporal evolution of the aCIN and the FPN nodes

The average ERPs for correct responses were used for the LORETA (Pascual-Marqui et al., 1994) to obtain the cortically localized sources of the aCIN and FPN. Fig. 4 shows the locations of peak source activity in the first row and the locations and orientations of fitted dipoles in the second row.

The activation in the nodes of aCIN started at ~76 ms after stimulus-onset. Maximum peak activation occurred at ~84 ms in the R AI and L AI, followed by peak activation in the DACC at ~98 ms. Dominant activation occurred in the right PPC at ~74 ms, and in the left DLPFC at ~224 ms. Beside those nodes, we also observed activation in the visual area (V_1) at ~60 ms, and in the ventral temporal cortex–fusiform face area (FFA) and para-hippocampal place area (PPA)–at ~160 ms (Fig S7). Table 1 lists the ERP source locations,

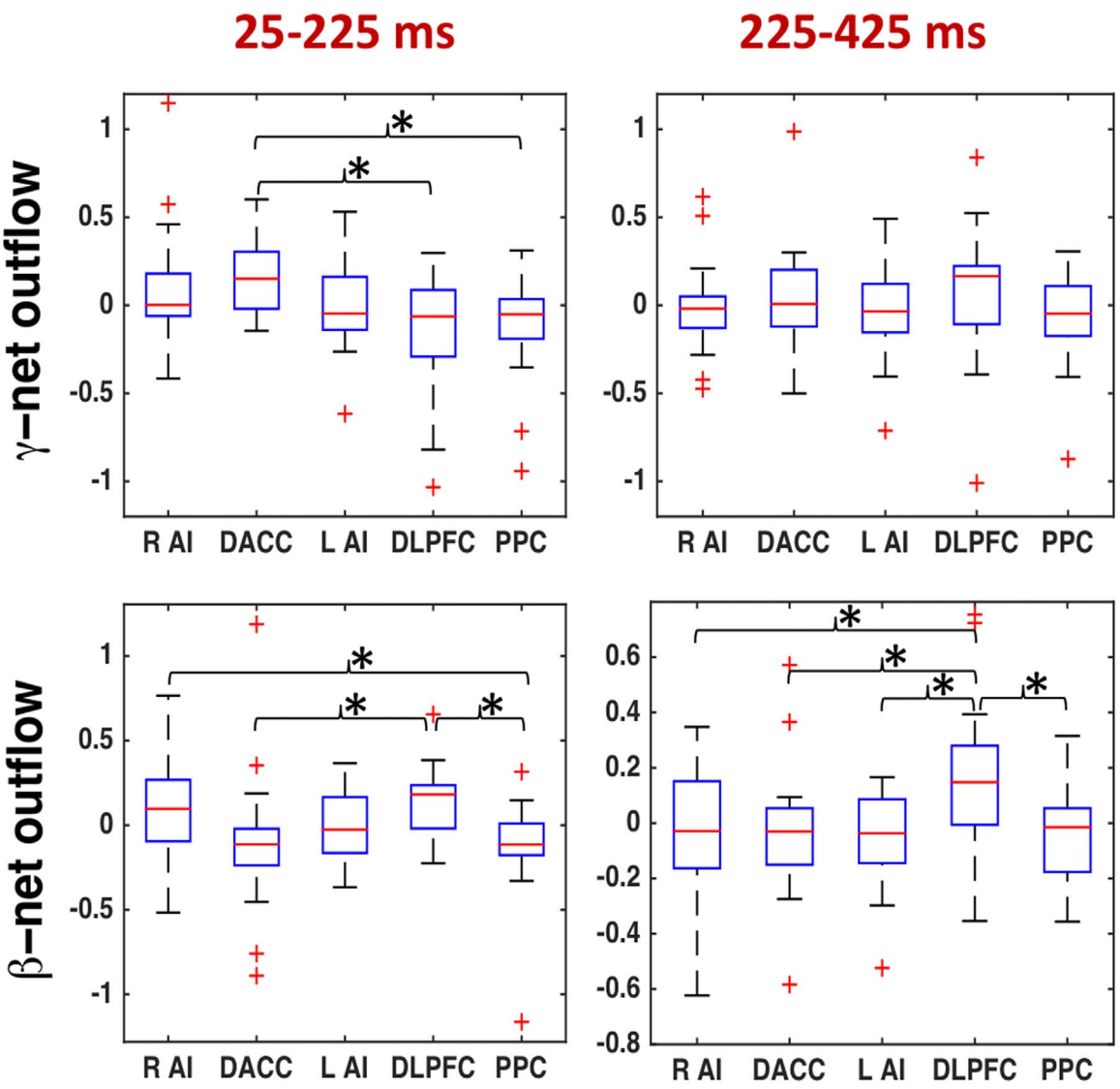

Fig. 5. Net Granger causal outflow at the right anterior insula (R AI), dorsal anterior cingulate cortex (DACC) and left anterior insula (L AI) nodes of the anterior cingulate-insula network (aCIN) and the dorsolateral prefrontal cortex (DLPFC) and posterior parietal cortex (PPC) nodes of the fronto-parietal network (FPN) for 0% noisy stimuli. The first row shows net outflow in gamma band in both timeframe 1 (25–225 ms) and timeframe 2 (225–425 ms) revealing that the aCIN controls over the FPN in timeframe 1. The second row shows net outflow in beta band in both timeframe 1 (25–225 ms) and timeframe 2 (225–425 ms) revealing that the FPN controls over the aCIN in timeframe 2 (* indicates significant p-value ($p < 0.05$; FDR-corrected)).

dipole orientations of the source model, and dominant activation timeframe of cortical sources. The fitted dipoles explained approximately 80% of the EEG signal. To test our hypotheses, we limited our study in the aCIN and FPN nodes.

Interactions between the aCIN and the FPN for clear images (easy task)

Spectral power computed at each node of the aCIN and the FPN showed peak activity in beta (~22 Hz) and gamma (~80 Hz) bands (Fig. S1). To assess the network interaction between the aCIN and the FPN, we computed Granger causality between all possible pairs of the nodes. We further computed the net Granger causal outflow (out-in) at each node of the aCIN and the FPN in both beta and gamma bands in both timeframes. We compared the net outflow among the nodes using Wilcoxon rank sum test followed by false discovery rate (FDR) (Benjamini and Hochberg, 1995) for multiple comparisons (timeframes and frequency bands) as shown in Fig. 5. In the gamma band, the net Granger causal outflow calculations at each node revealed that the aCIN node has a significantly higher net Granger causal outflow than that of the FPN node in the 25–225 ms timeframe ($p < 0.05$; FDR-corrected). The significantly higher outflow of the aCIN did not survive in the 225–425 ms timeframe. In the beta band, analysis of the net Granger causal outflow at each node demonstrated that the DLPFC of the FPN has a significantly higher net outflow than that of the aCIN nodes in later time 225–425 ms ($p < 0.05$; FDR-corrected). Granger causality node to node connectivity also showed consistent patterns (Fig. S8). We also the examined the interaction patterns of aCIN and FPN with the lower and higher visual areas (V1, FFA and PPA) in our analysis (Fig. S11 for 0% noisy stimuli). It turned out that the aCIN still controls over the FPN in timeframe 1 (25–225 ms) in gamma band and the DLPFC of FPN and/or the higher/lower visual areas control over the aCIN in timeframe 2 (225–425 ms) in beta band.

Interactions between the aCIN and the FPN for noisy images (difficult task)

Spectral power computed at each node of the aCIN and the FPN showed peak activity in beta (~22 Hz) and gamma (~80 Hz) bands also for 40% and 55% noisy stimuli (Figs. S2, S3). In both bands, the overall

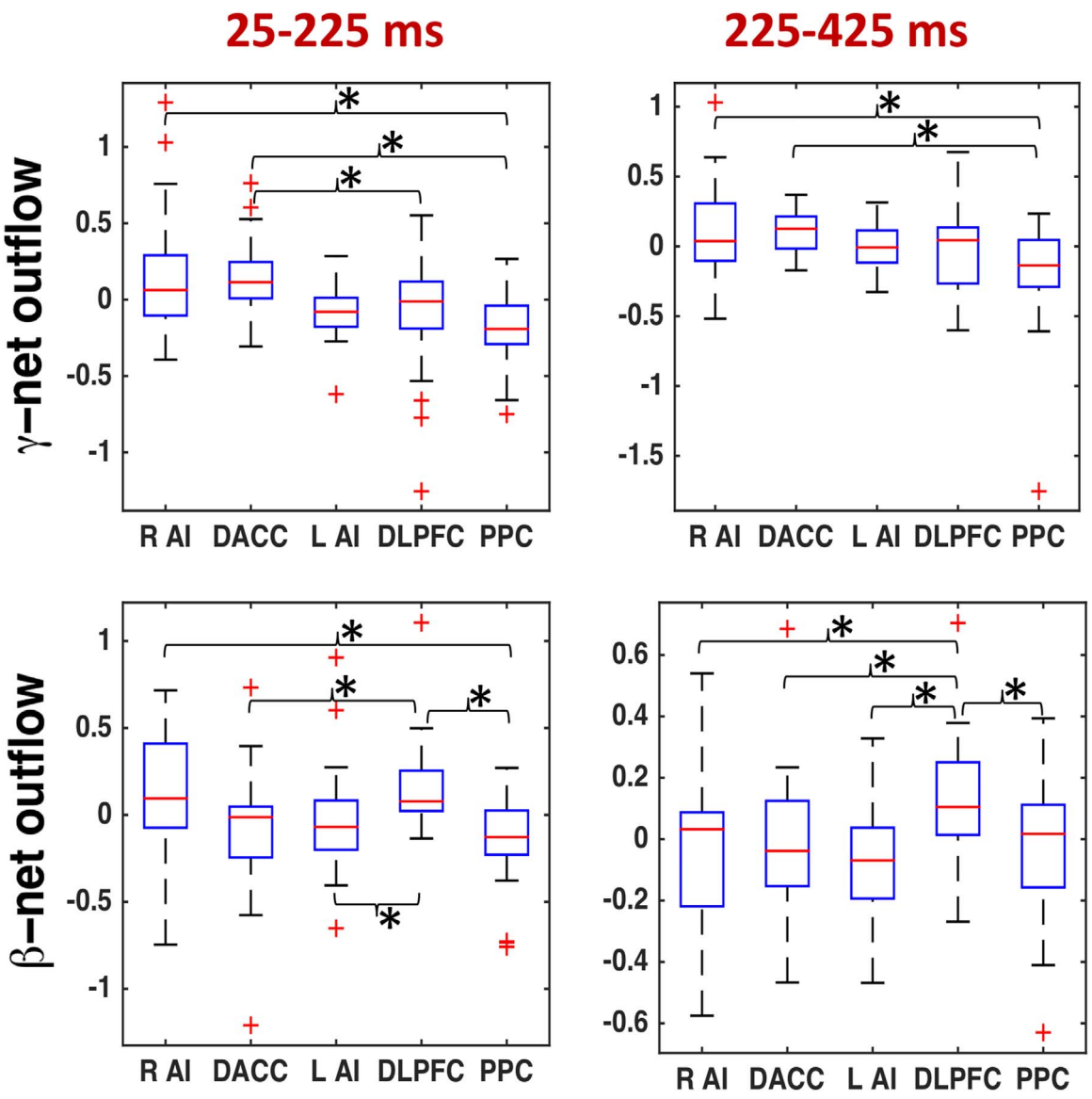

Fig. 6. Net Granger causal outflow at the right anterior insula (R AI), dorsal anterior cingulate cortex (DACC) and left anterior insula (L AI) nodes of the anterior cingulate-insula network (aCIN) and the dorsolateral prefrontal cortex (DLPFC) and posterior parietal cortex (PPC) nodes of the fronto-parietal network (FPN) for 40% noisy stimuli. The first row shows net outflow in gamma band in both timeframe 1 (25–225 ms) and timeframe 2 (225–425 ms) revealing that the aCIN controls over the FPN robustly in timeframe 1. The second row shows net outflow in beta band in both timeframe 1 (25–225 ms) and timeframe 2 (225–425 ms) revealing that the FPN controls over the aCIN in timeframe 2 (* indicates significant p-value ($p < 0.05$; FDR-corrected)).

spectral power increased with the increase in noise levels in the stimuli (Fig. S4). To assess the network interaction between the aCIN and the FPN nodes, we then computed Granger causality between all possible pairs of nodes for both noisy stimuli. We further computed the net Granger causal outflow (out-in) at each node of the aCIN and the FPN in both beta and gamma bands in each timeframe. We compared the net outflow among the nodes as shown in Figs. 6 and 7. In gamma band, the net Granger causal outflow calculations at each node revealed that the aCIN nodes have a significantly higher net outflow than that of the FPN nodes in the 25–225 ms timeframe ($p < 0.05$; FDR-corrected). In beta band, computations of the net outflow at each node uncovered that the FPN, especially the DLPFC, has a significantly higher net Granger causal outflow than that of the aCIN regions in 225–425 ms timeframe ($p < 0.05$; FDR-corrected). Granger causality node to node connectivity also demonstrated consistent patterns (Figs. S9, S10). When we included the V1, FFA and PPA into network analysis, the aCIN still initiated control over the FPN in timeframe 1 (25–225 ms) in gamma band and the DLPFC of FPN and/or the V1, FFA and PPA controlled over the aCIN in timeframe 2 (225–425 ms) in beta band (Figs. S12, S13).

We also computed Granger causality spectra using sliding window approach (Fig. S5), calculated outflow from each node, and averaged over time in two windows to examine the band-specific overall Granger causal outflow (Fig. S6). In the gamma band, the aCIN took control over the FPN in 25–225 ms, and remains the same till 225–425 ms (as reflected in 40% noise level: Fig. 6). In the beta-band, the FPN took control over the aCIN in 225–425 ms.

Discussion

Our analyses demonstrated that beta (~22 Hz) and gamma (~80 Hz) bands of neural activity involve between the aCIN and the FPN interactions for both easier and harder decisions. In behaviorally easier task, our gamma Granger causal outflow calculations in 25–225 ms indicated that the aCIN played a Granger causal control to the FPN consistent with previous fMRI studies (Goulden et al., 2014; Sridharan et al., 2008). In contrast, beta Granger causal outflow calculations further uncovered that the FPN played Granger causal control to the aCIN in 225–425 ms timeframe. Those band-specific

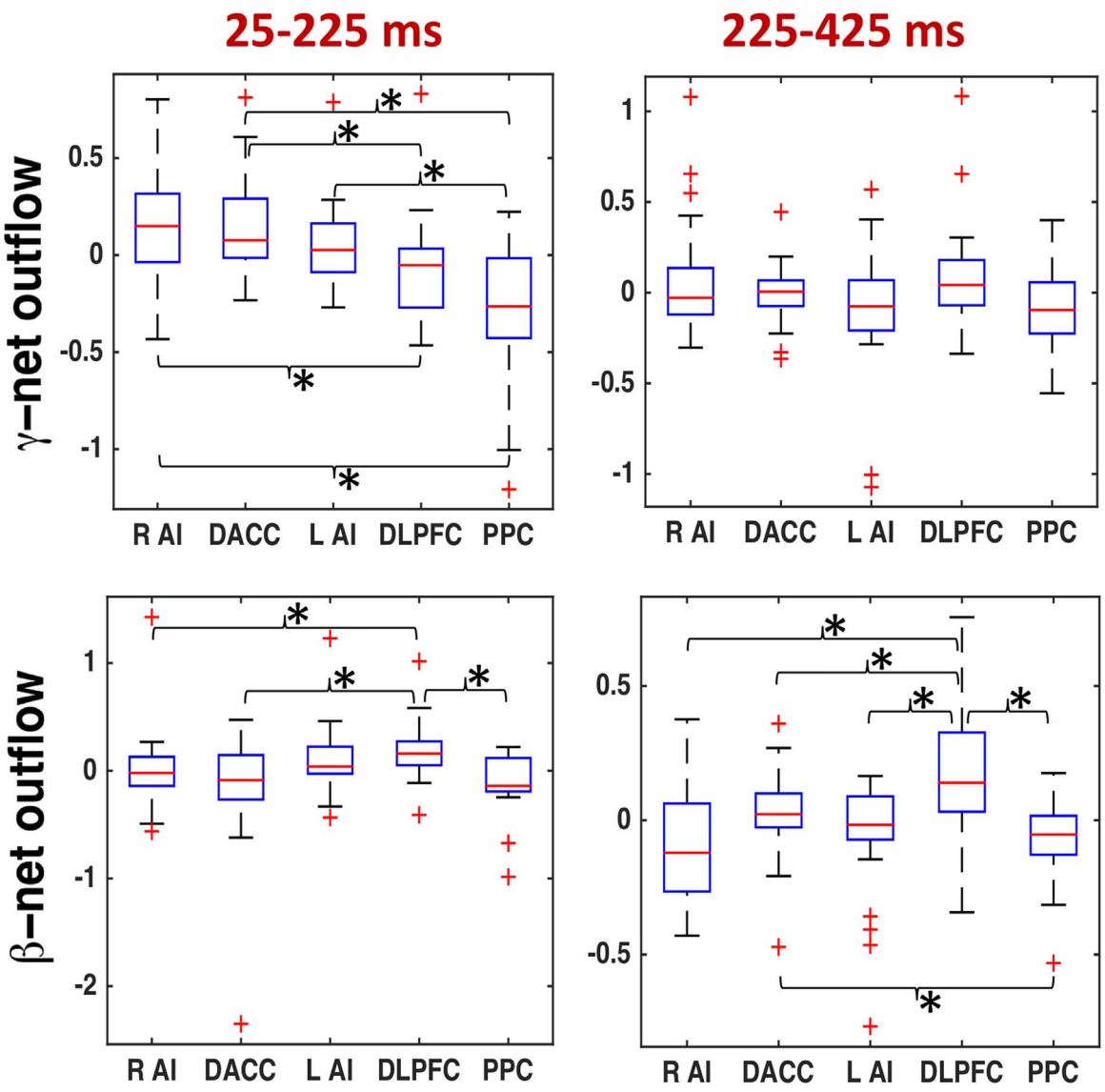

Fig. 7. Net Granger causal outflow at the right anterior insula (R AI), dorsal anterior cingulate cortex (DACC) and left anterior insula (L AI) nodes of the anterior cingulate-insula network (aCIN) and the dorsolateral prefrontal cortex (DLPFC) and posterior parietal cortex (PPC) nodes of the fronto-parietal network (FPN) for 55% noisy stimuli. The first row shows net outflow in gamma band in both timeframe 1 (25–225 ms) and timeframe 2 (225–425 ms) revealing that the aCIN controls over the FPN in timeframe 1. The second row shows net outflow in beta band in both timeframe1 (25–225 ms) and timeframe 2 (225–425 ms) revealing that the FPN controls over the aCIN in timeframe 2 (* indicates significant p-value ($p < 0.05$; FDR-corrected)).

time-dependent Granger causal outflow features of the aCIN and the FPN were also retained for behaviorally harder decision-making tasks.

Gamma band control

Electrophysiological studies suggested that gamma band activity is associated with a wide range of cognitive processes (Buzsaki and Wang, 2012; Fries, 2009; Jensen et al., 2007; Senkowski et al., 2008), including the attentional selection of relevant visual inputs during sensory processing (Hipp et al., 2011; Siegel et al., 2011). The fMRI studies have demonstrated that the aCIN drives the FPN and other network such as the default-mode (Chand and Dhamala, 2016a; Goulden et al., 2014; Sridharan et al., 2008). The AI and DACC are anatomically a part of network and integrate information from multiple brain regions (Critchley et al., 2004). The von Economo neurons (VENs)–special type of neurons exclusively localized to the AI and ACC–relay information processed within these regions to other parts of the brain (Allman et al., 2005; Watson et al., 2006). The control signals generated by the AI and DACC might be supported by the neuronal basis of control signals of the VENs. Many previous studies of attention and cognitive control have reported co-activation of the AI and DACC (Crottaz-Herbette and Menon, 2006; Dosenbach et al., 2006; Ham et al., 2013). Activity in the DACC is known to signal the need for enhanced cognitive control (Egner, 2009; Ridderinkhof et al., 2004). Electrophysiological studies suggest that the DACC provides the first cortical signal for salient events (Debener et al., 2005; Dehaene et al., 1994). The AI is functionally connected to the networks responsible for adaptive behavior, including the salience network (Seeley et al., 2007), as well as other parts of the fronto-parietal control network (Vincent et al., 2008). This cortical area has direct white matter connections to other key regions, including the DACC (van den Heuvel et al., 2009), inferior-parietal lobe (Uddin et al., 2010), and temporo-parietal junction (Kucyi et al., 2012) making the insula well placed to perform its putative role of evaluating (Eckert et al., 2009), reorienting attention (Ullsperger et al., 2010), and switching between cognitive resources in response to salient events (Uddin and Menon, 2009). Our findings and existing literature taken together thus might indicate that the gamma band aCIN (i.e., DACC-AI network) initiates control signals for relevant sensory selection of visual inputs.

Beta band control

Prior studies demonstrated that beta oscillation is associated with motor functions (Baker, 2007; Chakarov et al., 2009; Davis et al., 2012; Klostermann et al., 2007; Riddle and Baker, 2006) and is involved in maintaining better accuracy in decision-making (Hipp et al., 2011; Siegel et al., 2011). The beta band results showed that the DLPFC acted Granger causal control over the PPC and aCIN nodes in 225–425 ms timeframe. The role of DLPFC has been illustrated consistently for actively maintaining and manipulating information in working memory and for goal-oriented behavior such as decision-making (Koechlin and Summerfield, 2007; Menon, 2011; Muller and Knight, 2006; Petrides, 2005). Anatomical studies have provided the evidence that DLPFC and sensory areas have rich connections (Miller and Cohen, 2001). The DLPFC receives visual, somatosensory, and auditory sensory inputs from the occipital, parietal, and temporal cortices (Petrides and Pandya, 1999), and its anatomical connections with pre-motor/motor areas further support to achieve the motor outputs (Lu et al., 1994). Our beta band results supported the putative role of the DLPFC for top-down processing (Miller and Cohen, 2001). Electrophysiological studies (Hipp et al., 2011; Siegel et al., 2012; Siegel et al., 2011) also reported that beta band activity of the DLPFC (of the FPN) is important in linking sensory evidence to motor plans. This beta band control in later time (225–425 ms) thus might indicate the active maintenance of past evidence during its accumulation in coordination with V1, FFA and PPA and/or its flexible routing to motor plans.

In summary, the present study evaluated the aCIN and FPN, with regards to the temporal evolution of averaged evoked potentials in the nodes and oscillatory networks that organized evoked activity between the aCIN and the FPN. We found that the beta band (~22 Hz) and gamma (~80 Hz) bands of neural activity involved between the aCIN and FPN interactions. The aCIN activity initiated the Granger causal control over the FPN activity in 25–225 ms in gamma band and the FPN activity achieved the control over the aCIN activity in 225–425 ms in beta band for both easier and harder decision-making tasks. These findings provide important insights into how sensory information enters and organizes between the aCIN and the FPN during sensory-guided goal-directed behaviors such as perceptual decision-making.

Acknowledgements

This work was financially supported by a National Science Foundation CAREER award to MD (BCS 0955037).

Appendix A. Supporting information

Supplementary data associated with this article can be found in the online version at doi:10.1016/j.neuroimage.2017.03.014.

References

Adhikari, B.M., Sathian, K., Epstein, C.M., Lamichhane, B., Dhamala, M., 2014. Oscillatory activity in neocortical networks during tactile discrimination near the limit of spatial acuity. Neuroimage 91, 300–310.
Allman, J.M., Watson, K.K., Tetreault, N.A., Hakeem, A.Y., 2005. Intuition and autism: a possible role for Von Economo neurons. Trends Cogn. Sci. 9, 367–373.
Bajaj, S., Adhikari, B.M., Friston, K.J., Dhamala, M., 2016. Bridging the gap: dynamic causal modeling and Granger causality analysis of resting state fMRI. Brain Connect.
Baker, S.N., 2007. Oscillatory interactions between sensorimotor cortex and the periphery. Curr. Opin. Neurobiol. 17, 649–655.
Benjamini, Y., Hochberg, Y., 1995. Controlling the false discovery rate: a practical and powerful approach to multiple testing. J R. Stat. Soc. B (Methodol.), 289–300.
Bonnelle, V., Ham, T.E., Leech, R., Kinnunen, K.M., Mehta, M.A., Greenwood, R.J., Sharp, D.J., 2012. Salience network integrity predicts default mode network function after traumatic brain injury. Proc. Natl. Acad. Sci. USA 109, 4690–4695.
Buzsaki, G., Wang, X.J., 2012. Mechanisms of gamma oscillations. Annu. Rev. Neurosci. 35, 203–225.
Chakarov, V., Naranjo, J.R., Schulte-Monting, J., Omlor, W., Huethe, F., Kristeva, R., 2009. Beta-range EEG-EMG coherence with isometric compensation for increasing modulated low-level forces. J. Neurophysiol. 102, 1115–1120.
Chand, G.B., Dhamala, M., 2014. Spectral factorization-based current source density analysis of ongoing neural oscillations. J. Neurosci. Methods 224, 58–65.
Chand, G.B., Dhamala, M., 2016a. Interactions among the brain default-mode, salience, and central-executive networks during perceptual decision-making of moving dots. Brain Connect 6 (3), 249–254.
Chand, G.B., Dhamala, M., 2016b. The salience network dynamics in perceptual decision-making. Neuroimage 134, 85–93.
Chand, G.B., Lamichhane, B., Dhamala, M., 2016. Face or house image perception: beta and gamma bands of oscillations in brain networks carry out decision-making. Brain Connect 6 (8), 621–631.
Chen, A.C., Oathes, D.J., Chang, C., Bradley, T., Zhou, Z.W., Williams, L.M., Glover, G.H., Deisseroth, K., Etkin, A., 2013. Causal interactions between fronto-parietal central executive and default-mode networks in humans. Proc. Natl. Acad. Sci. USA 110, 19944–19949.
Clemens, B., Bessenyei, M., Fekete, I., Puskas, S., Kondakor, I., Toth, M., Hollody, K., 2010. Theta EEG source localization using LORETA in partial epilepsy patients with and without medication. Clin. Neurophysiol. 121, 848–858.
Critchley, H.D., Wiens, S., Rotshtein, P., Ohman, A., Dolan, R.J., 2004. Neural systems supporting interoceptive awareness. Nat. Neurosci. 7, 189–195.
Crottaz-Herbette, S., Menon, V., 2006. Where and when the anterior cingulate cortex modulates attentional response: combined fMRI and ERP evidence. J. Cogn. Neurosci. 18, 766–780.
Cui, J., Xu, L., Bressler, S.L., Ding, M., Liang, H., 2008. BSMART: a Matlab/C toolbox for analysis of multichannel neural time series. Neural Netw. 21, 1094–1104.
Dale, A.M., Sereno, M.I., 1993. Improved localization of cortical activity by combining EEG and MEG with MRI cortical surface reconstruction: a linear approach. J. Cogn. Neurosci. 5, 162–176.
Davis, N.J., Tomlinson, S.P., Morgan, H.M., 2012. The role of beta-frequency neural oscillations in motor control. J. Neurosci. 32, 403–404.
Debener, S., Ullsperger, M., Siegel, M., Fiehler, K., von Cramon, D.Y., Engel, A.K., 2005. Trial-by-trial coupling of concurrent electroencephalogram and functional magnetic resonance imaging identifies the dynamics of performance monitoring. J. Neurosci. 25, 11730–11737.
Deco, G., Jirsa, V.K., McIntosh, A.R., 2011. Emerging concepts for the dynamical organization of resting-state activity in the brain. Nat. Rev. Neurosci. 12, 43–56.
Dehaene, S., Posner, M.I., Tucker, D.M., 1994. Localization of a neural system for error-detection and compensation. Psychol. Sci. 5, 303–305.
Dhamala, M., 2014. Spectral interdependency methods. Enclyclopedia Comput. Neurosci., 1–6.
Dhamala, M., Rangarajan, G., Ding, M., 2008a. Analyzing information flow in brain networks with nonparametric Granger causality. Neuroimage 41, 354–362.
Dhamala, M., Rangarajan, G., Ding, M., 2008b. Estimating granger causality from fourier and wavelet transforms of time series data. Phys. Rev. Lett. 100.
Diener, C., Kuehner, C., Brusniak, W., Ubl, B., Wessa, M., Flor, H., 2012. A meta-analysis of neurofunctional imaging studies of emotion and cognition in major depression. Neuroimage 61, 677–685.
Ding, M., Bressler, S.L., Yang, W., Liang, H., 2000. Short-window spectral analysis of cortical event-related potentials by adaptive multivariate autoregressive modeling: data preprocessing, model validation, and variability assessment. Biol. Cybern. 83, 35–45.
Dosenbach, N.U., Visscher, K.M., Palmer, E.D., Miezin, F.M., Wenger, K.K., Kang, H.C., Burgund, E.D., Grimes, A.L., Schlaggar, B.L., Petersen, S.E., 2006. A core system for the implementation of task sets. Neuron 50, 799–812.
Eckert, M.A., Menon, V., Walczak, A., Ahlstrom, J., Denslow, S., Horwitz, A., Dubno, J.R., 2009. At the heart of the ventral attention system: the right anterior insula. Hum. Brain Mapp. 30, 2530–2541.
Egner, T., 2009. Prefrontal cortex and cognitive control: motivating functional hierarchies. Nat. Neurosci. 12, 821–822.
Ekman, P., Friesen, W.V., 1976. Pictures of Facial Affect. Consulting Psychologists Press, Palo Alto (CA).
Fries, P., 2009. Neuronal gamma-band synchronization as a fundamental process in cortical computation. Annu Rev. Neurosci. 32, 209–224.
Goulden, N., Khusnulina, A., Davis, N.J., Bracewell, R.M., Bokde, A.L., McNulty, J.P., Mullins, P.G., 2014. The salience network is responsible for switching between the default mode network and the central executive network: replication from DCM. Neuroimage 99, 180–190.
Haalman, I., Vaadia, E., 1997. Dynamics of neuronal interactions: relation to behavior, firing rates, and distance between neurons. Hum. Brain Mapp. 5, 249–253.
Ham, T., Leff, A., de Boissezon, X., Joffe, A., Sharp, D.J., 2013. Cognitive control and the salience network: an investigation of error processing and effective connectivity. J. Neurosci. 33, 7091–7098.
Hämäläinen, M., Hari, R., Ilmoniemi, R.J., Knuutila, J., Lounasmaa, O.V., 1993. Magnetoencephalography-theory, instrumentation, and applications to noninvasive studies of the working human brain. Rev. Mod. Phys. 65, 413–497.
Heekeren, H.R., Marrett, S., Bandettini, P.A., Ungerleider, L.G., 2004. A general mechanism for perceptual decision-making in the human brain. Nature 431, 859–862.
Heekeren, H.R., Marrett, S., Ungerleider, L.G., 2008. The neural systems that mediate human perceptual decision making. Nat. Rev. Neurosci. 9, 467–479.
Herrmann, M.J., Ehlis, A.C., Muehlberfer, A., Fallgatter, A.J., 2005. Source localization of early stages of face processing. Brain Topogr. 18, 77–85.
van den Heuvel, M.P., Mandl, R.C., Kahn, R.S., Hulshoff Pol, H.E., 2009. Functionally linked resting-state networks reflect the underlying structural connectivity architecture of the human brain. Hum. Brain Mapp. 30, 3127–3141.
Hipp, J.F., Engel, A.K., Siegel, M., 2011. Oscillatory synchronization in large-scale cortical networks predicts perception. Neuron 69, 387–396.

Jensen, O., Kaiser, J., Lachaux, J.P., 2007. Human gamma-frequency oscillations associated with attention and memory. Trends Neurosci. 30, 317–324.
Jones, R., Bhattacharya, J., 2012. Alpha activity in the insula accompanies the urge to neutralize in sub-clinical obsessive-compulsive participants. J. Behav. Addict. 1, 96–105.
Junghofer, M., Elbert, T., Tucker, D.M., Rockstroh, B., 2000. Statistical control of artifacts in dense array EEG/MEG studies. Psychophysiol 37, 523–532.
Klostermann, F., Nikulin, V.V., Kuhn, A.A., Marzinzik, F., Wahl, M., Pogosyan, A., Kupsch, A., Schneider, G.H., Brown, P., Curio, G., 2007. Task-related differential dynamics of EEG alpha- and beta-band synchronization in cortico-basal motor structures. Eur. J. Neurosci. 25, 1604–1615.
Koechlin, E., Summerfield, C., 2007. An information theoretical approach to prefrontal executive function. Trends Cogn. Sci. 11, 229–235.
Kucyi, A., Moayedi, M., Weissman-Fogel, I., Hodaie, M., Davis, K.D., 2012. Hemispheric asymmetry in white matter connectivity of the temporoparietal junction with the insula and prefrontal cortex. PLoS One 7, e35589.
Lu, M.-T., Preston, J.B., Strick, P.L., 1994. Interconnections between the prefrontal cortex and the premotor areas in the frontal lobe. J. Com. Neurol. 341, 375–392.
Menon, V., 2011. Large-scale brain networks and psychopathology: a unifying triple network model. Trends Cogn. Sci. 15, 483–506.
Menon, V., Uddin, L.Q., 2010. Saliency, switching, attention and control: a network model of insula function. Brain Struct. Funct. 214, 655–667.
Michel, C.M., Murray, M.M., Lantz, G., Gonzalez, S., Spinelli, L., Grave de Peralta, R., 2004. EEG source imaging. Clin. Neurophysiol. 115, 2195–2222.
Miller, E.K., Cohen, J.D., 2001. An integrative theory of pretrontal cortex function. Annu. Rev. Neurosci. 24, 167–202.
Muller, N.G., Knight, R.T., 2006. The functional neuroanatomy of working memory: contributions of human brain lesion studies. Neuroscience 139, 51–58.
Nguyen, V.T., Breakspear, M., Cunnington, R., 2014. Fusing concurrent EEG-fMRI with dynamic causal modeling: application to effective connectivity during face perception. Neuroimage 102 (Pt 1), 60–70.
Painold, A., Anderer, P., Holl, A.K., Letmaier, M., Saletu-Zyhlarz, G.M., Saletu, B., Bonelli, R.M., 2011. EEG low-resolution brain electromagnetic tomography (LORETA) in Huntington's disease. J Neurol. 258, 840–854.
Pascual-Marqui, R.D., Michel, C.M., Lehmann, D., 1994. Low resolution electromagnetic tomography: a new method for localizing electrical activity in the brain. Int. J. Psychophysiol., 49–65.
Pascual-Marqui, R.D., Lehmann, D., Koenig, T., Kochi, K., Merlo, M.C.G., Hell, D., Koukkou, M., 1999. Low resolution brain electromagnetic tomography (LORETA) functional imaging in acute, neuroleptic-naive, first-episode, productive schizophrenia. Psychiatry Res. Neuroimaging 90, 169–479.
Petrides, M., 2005. Lateral prefrontal cortex: architectonic and functional organization. Philos. Trans. R. Soc. Lond. B Biol. Sci. 360, 781–795.
Petrides, M., Pandya, D.N., 1999. Dorsolateral prefrontal cortex: comparative cytoarchitectonic analysis in the human and the macaque brain and corticocortical connection patterns. Eur. J. Neurosci. 11, 1011–1036.
Power, J.D., Cohen, A.L., Nelson, S.M., Wig, G.S., Barnes, K.A., Church, J.A., Vogel, A.C., Laumann, T.O., Miezin, F.M., Schlaggar, B.L., Petersen, S.E., 2011. Functional network organization of the human brain. Neuron 72, 665–678.
Ridderinkhof, K.R., Ullsperger, M., Crone, E.A., Nieuwenhuis, S., 2004. The role of the medial frontal cortex in cognitive control. Science 306, 443–447.
Riddle, C.N., Baker, S.N., 2006. Digit displacement, not object compliance, underlies task dependent modulations in human corticomuscular coherence. Neuroimage 33, 618–627.
Rousselet, G.A., Husk, J.S., Bennett, P.J., Sekuler, A.B., 2008. Time course and robustness of ERP object and face differences. J. Vis. 8 (3), 1–18.
Seeley, W.W., Menon, V., Schatzberg, A.F., Keller, J., Glover, G.H., Kenna, H., Reiss, A.L., Greicius, M.D., 2007. Dissociable intrinsic connectivity networks for salience processing and executive control. J. Neurosci. 27, 2349–2356.
Senkowski, D., Schneider, T.R., Foxe, J.J., Engel, A.K., 2008. Crossmodal binding through neural coherence: implications for multisensory processing. Trends Neurosci. 31, 401–409.
Siegel, M., Engel, A.K., Donner, T.H., 2011. Cortical network dynamics of perceptual decision-making in the human brain. Front. Hum. Neurosci. 5, 21.
Siegel, M., Donner, T.H., Engel, A.K., 2012. Spectral fingerprints of large-scale neuronal interactions. Nat. Rev. Neurosci. 13, 121–134.
Sridharan, D., Levitin, D.J., Menon, V., 2008. A critical role for the right fronto-insular cortex in switching between central-executive and default-mode networks. Proc. Natl. Acad. Sci. USA 105, 12569–12574.
Thatcher, R.W., North, D.M., Biver, C.J., 2014. LORETA EEG phase reset of the default mode network. Front. Hum. Neurosci. 8, 529.
Uddin, L.Q., 2015. Salience processing and insular cortical function and dysfunction. Nat. Rev. Neurosci. 16, 55–61.
Uddin, L.Q., Menon, V., 2009. The anterior insula in autism: under-connected and under-examined. Neurosci. Biobehav. Rev. 33, 1198–1203.
Uddin, L.Q., Supekar, K., Amin, H., Rykhlevskaia, E., Nguyen, D.A., Greicius, M.D., Menon, V., 2010. Dissociable connectivity within human angular gyrus and intraparietal sulcus: evidence from functional and structural connectivity. Cereb. Cortex 20, 2636–2646.
Ullsperger, M., Harsay, H.A., Wessel, J.R., Ridderinkhof, K.R., 2010. Conscious perception of errors and its relation to the anterior insula. Brain Struct. Funct. 214, 629–643.
Velikova, S., Locatelli, M., Insacco, C., Smeraldi, E., Comi, G., Leocani, L., 2010. Dysfunctional brain circuitry in obsessive-compulsive disorder: source and coherence analysis of EEG rhythms. Neuroimage 49, 977–983.
Vincent, J.L., Kahn, I., Snyder, A.Z., Raichle, M.E., Buckner, R.L., 2008. Evidence for a frontoparietal control system revealed by intrinsic functional connectivity. J Neurophysiol. 100, 3328–3342.
Watson, K.K., Jones, T.K., Allman, J.M., 2006. Dendritic architecture of the von Economo neurons. Neuroscience 141, 1107–1112.